Int. J. Appl. Math. Comput. Sci., 2020, Vol. 30, No. 2, 351–361
DOI: 10.34768/amcs-2020-0027

SOLUTION OF AN INVERSE KINEMATICS PROBLEM USING DUAL QUATERNIONS

LEI CHEN [a], TERESA ZIELINSKA [b], JIKUN WANG [c], WEIMIN GE [a,d,*]

[a]Tianjin Key Laboratory for Advanced Mechatronic Systems Design and Intelligent Control
Tianjin University of Technology
No. 391 Bin Shui Xi Dao Road, Xiqing District, Tianjin 300384, China
e-mail: geweimin@email.tjut.edu.cn

[b]Institute of Aeronautics and Applied Mechanics, Faculty of Power and Aeronautical Engineering
Warsaw University of Technology
ul. Nowowiejska 24, 00-665 Warsaw, Poland

[c]Institute of Automatic Control and Robotics, Faculty of Mechatronics
Warsaw University of Technology
ul. św. Andrzeja Boboli 8, 02-525 Warsaw, Poland

[d]National Demonstration Center for Experimental Mechanical and Electrical Engineering Education
Tianjin University of Technology
No. 391 Bin Shui Xi Dao Road, Xiqing District, Tianjin 300384, China

The paper proposes a solution to an inverse kinematics problem based on dual quaternions algebra. The method, relying on screw theory, requires less calculation effort compared with commonly used approaches. The obtained kinematic description is very concise, and the singularity problem is avoided. The dual quaternions formalism is applied to the problem decomposition and description. As an example, the kinematics problem of a multi-DOF serial manipulator is considered. Direct and inverse kinematics problems are solved using division into sub-problems. Each new sub-problem proposed is concerned with rotation about two subsequent axes by a given amount. The presented example verifies the correctness and feasibility of the proposed approach.

Keywords: dual quaternions, kinematics, simulation, robotics, screw theory.

1. Introduction

Efficient solution of inverse kinematics problems is essential for real-time control of robotic manipulators. In real-time control, the end-effector trajectory is generated on-line considering the manipulator task and current sensory readings. Considering the needed end-effector position, joints positions are calculated using inverse kinematics equations. Such an operation must be performed extremely fast with a minimal delay of the robot reaction to the recently obtained sensory readings. The proposed approach provides an organized and pre-defined method of solving the inverse kinematics problem. The solution requires fewer computations, and the delivered set of equations is less complex than the one obtained analytically using the Denavit–Hartenberg (D–H) approach.

At present, kinematic structures are mainly described using the D–H formalism (Zhu and Zhao, 2019; Singh *et al.*, 2018) or the screw theory formalism (Chang *et al.*, 2018; Xiong *et al.*, 2017). The D–H formalism requires a proper definition of the coordinate system. Here the inverse kinematics problem can be solved in many ways. Often, researchers apply the Jacobian-based approach using different types of matrix pseudo-inverses. In this approach, the motion, but not the position of the end-effector, is transformed into the motion of

*Corresponding author

internal coordinates. Therefore, in robot controllers, the position and orientation must be obtained considering the formula for discrete integration, which introduces numerical approximation. Hence, if at each time moment, accurate positioning of the manipulator is relevant, the Jacobian-based approach is not the best option.

In another approach, the solution to the inverse kinematics problem is obtained analytically using the formulas for a direct problem (e.g., with the D–H formalism). Such an approach delivers complex equations even for rather simple serial structures, and in the end it requires solution of sets of conditioned trigonometric equations. Another possibility is to intuitively analyze the manipulator geometry delivering inverse kinematics equations (Craig, 2009). Here the solution plan is not uniform and can be easily affected by mistakes. In both cases, singularity causes a problem and must be managed separately. Therefore, researchers are still searching for methods with clearer algorithmic schemes and simpler transformations. These include methods using screw theory and dual quaternions (Kenwrigth, 2013). Screw theory avoids singularities. It uses the product of exponentials (POE) and quaternions algebra as a major formal tool. Solving inverse kinematics problems based on screw theory requires appropriate decomposition to sub-problems (Murray, 1994). A method based on decomposition to sub-problems brings a clear geometric meaning (Sariyildiz and Temeltas, 2012).

Currently, the solution of inverse kinematics often applies the Paden–Kahan sub-problem formulation. Unfortunately, the method cannot support inverse kinematics solutions for all configurations. If there are no crossing axes in the configuration, it will not work. Yue-sheng and Ai-Ping (2008) proposed a sub-problems-based method valid for kinematic structures which have separated axes. The method is, however, still insufficient to solve the inverse kinematics problem for a 6DOF manipulator when its structure includes at least two non-intersecting axes.

Some researchers proposed sub-problems for solving cases with three parallel rotating axes. Zhao *et al*. (2018) introduced a new sub-problems-based method which uses POE. They solved the inverse kinematics problem for a configuration with three parallel axes. Chen *et al*. (2015) solved the inverse kinematics problem using the sub-problems approach for the case where three axes do not intersect and two of them are parallel in the same plane. The method was applied to a typical 6DOF manipulator. Recently, many researchers have been exploring screw theory methods further. An *et al.* (2018; 2017) provided a new method for analyzing the motion of a manipulator. A concept of mutual moments was also introduced. Wang *et al*. (2018) proposed a method for solving the inverse kinematics problem of an arbitrary 3R manipulator (manipulator with three revolute joints) using the POE model and Rodrigues formula. However, the POE method is not universal enough.

It is obvious that numerical precision and real-time calculations efficiency are very relevant for robot control systems. Having the above in mind, it was decided to develop a new approach to solving the inverse kinematics problem using dual quaternions (Clifford, 1882), i.e., the kinematic transformation method, which is numerically efficient. The dual quaternions approach provides a simple form for a rigid body description (Kussaba *et al.*, 2017; Wang *et al.*, 2013; 2012). It has been widely used for motion tracking in aeronautics (Gui and Vukovich, 2016) and for mapping (Mueller, 2017), but it is less explored for solving kinematics problems in robotics. Gouasmi *et al*. (2012) and Vidaković *et al*. (2014) proved benefits of kinematic modeling using the dual quaternions space. They compared formalisms (Euler angles, axis-angles, unit quaternions, dual quaternions, homogeneous transformations, etc.) used for kinematic analysis of rigid bodies including serial manipulators. Oezguer and Mezouar (2016) described the kinematics of a manipulator using dual quaternions. Sariyildiz *et al*. (2011) analyzed forward and inverse kinematics problems for a 6DOF manipulator using three methods: quaternions algebra, exponential mapping method and dual quaternions. Cariow *et al*. (2015) elaborated and implemented a method which improves the computational efficiency of dual quaternions operations. The obtained results indicated that dual quaternions provide a compact and computationally efficient solution.

Based on state-of-the-art knowledge, it must be concluded that it is very beneficial to apply dual quaternions in the field of robotics. In this paper, a general method based on dual quaternions and Plücker coordinates is applied using decomposition to sub-problems known from the literature. Applying the quaternion, multi-degree-of-freedom manipulator kinematics are divided into parts described by the corresponding sub-problems. The solution of the inverse kinematics problem for a multi-DOF manipulator is obtained in steps, and mathematical operations are simplified. The presented studies deliver a novel formalization of the sub-problem, based on the dual quaternions describing rotation about two subsequent axes for a given amount. Such transformation supports the inverse kinematics problem solution for a 3R structure with two intersecting axes and one which is separated. As a proof of concept, this method was applied to solving the inverse kinematics problem for a 6DOF manipulator with an atypical structure.

Section 2 presents the basics of the dual quaternions formalism and Plücker coordinates. Section 3 derives the new sub-problem and presents its general description. In Section 4 a novel structure of a 6DOF manipulator is analyzed using the proposed method. Section 5 presents

simulation results for the inverse kinematics problem, with an evaluation of computational efficiency. Section 7 concludes the paper and summarizes future research suggestions.

The presented method was preliminarily described by Ge *et al.* (2018; 2019). The current version covers an improved and expanded formulation and expanded case studies. Our previous papers (Ge *et al.*, 2018; 2019) were prepared at an earlier stage of the research. The new elements of the current work include (i) a detailed and systematic description of the method fundamentals with improved graphical illustrations (Sections 2 and 3), (ii) a comprehensive presentation of the elaborated procedure for solving the inverse kinematics problems using the dual quaternions method (Section 4), (iii) expanded testing examples (Section 5).

2. Mathematical preliminaries

Notation:
$\vec{(\cdot)}$ denotes the direction vector,
$\hat{(\cdot)}$ denotes the dual quaternion,
$\hat{(\cdot)}^*$ denotes the conjugate element of the quaternion,
$\hat{(\cdot)} \circ \hat{(\cdot)}$ denotes the product of the dual quaternion,
$\|(\cdot)\|$ denotes the Euclidean norm,
${}^{1n}\hat{(\cdot)}_R$ denotes the transformation of a rigid body; the second element of the left superscript ^{1n} is the transformation stage,
$S(\cdot)$ denotes the scalar part of the dual quaternion,
$\boldsymbol{V}(\cdot)$ denotes the vector part of the dual quaternion,
$SD\{\cdot\}$ denotes the scalar part in the dual part of the dual quaternion,
$SR\{\cdot\}$ denotes the scalar part in the real part of the dual quaternion,
$\boldsymbol{VD}\{\cdot\}$ denotes the vector part in the dual part of the dual quaternion,
$\boldsymbol{VR}\{\cdot\}$ denotes the vector part in the real part of the dual quaternion.

The quaternion is represented as the sum of a real and an imaginary part, in which the latter behaves as a vector,

$$\boldsymbol{q} = q_0 + q_1\vec{i} + q_2\vec{j} + q_3\vec{k} = (q_0, \boldsymbol{q}_V), \tag{1}$$

where q_0 is a scalar and $\boldsymbol{q}_V = [q_1, q_2, q_3]$ is a vector. The dual quaternion is expressed as the sum of two quaternions:

$$\hat{\boldsymbol{q}} = \boldsymbol{q}_S + \varepsilon\boldsymbol{q}_V = (\boldsymbol{q}_S, \boldsymbol{q}_V), \tag{2}$$

where $\boldsymbol{q}_S$ is the real part and $\boldsymbol{q}_V$ is the dual part, and ε is a dual factor. The real part represents the rotation, and the dual part represents the translation. According to (1), each $\hat{\boldsymbol{q}}_S$, $\hat{\boldsymbol{q}}_V$ consists of the scalar part ($SR\{\boldsymbol{q}_S\}$, $SD\{\boldsymbol{q}_V\}$) and the vector part ($\boldsymbol{VR}\{\boldsymbol{q}_S\}$, $\boldsymbol{VD}\{\boldsymbol{q}_V\}$), therefore $S(\hat{\boldsymbol{q}}) = SR\{\boldsymbol{q}_S\} + SD\{\boldsymbol{q}_V\}$ and $\boldsymbol{V}(\hat{\boldsymbol{q}}) = \boldsymbol{VR}\{\boldsymbol{q}_S\} + \boldsymbol{VD}\{\boldsymbol{q}_V\}$. The dual quaternion describes the screw type motion of a rigid body. The motion of a rigid body which is first translated and next rotated is represented by the dual quaternion as

$$\hat{\boldsymbol{q}} = \hat{\boldsymbol{q}}_T \circ \hat{\boldsymbol{q}}_R = \left(1 + \frac{\varepsilon}{2}\hat{\boldsymbol{q}}_T\right) \circ \hat{\boldsymbol{q}}_R. \tag{3}$$

The dual quaternion can be defined as an operator (Mukundan, 2002; Tan and Balchen, 1993), and the formula (3) can be rewritten as

$$\hat{\boldsymbol{q}} = \begin{bmatrix} \cos(\frac{\theta}{2}) \\ \sin(\frac{\theta}{2})\vec{r} \end{bmatrix} + \varepsilon \begin{bmatrix} -\frac{k}{2}\sin(\frac{\theta}{2}) \\ \sin(\frac{\theta}{2})\vec{m} + \frac{k}{2}\cos(\frac{\theta}{2})\vec{r} \end{bmatrix}, \tag{4}$$

where θ is the rotation angle about the screw axis, $\vec{r}$ is the direction of screw axis, k is the translation along the screw axis, $\vec{m}$-is the moment of the screw axis (obtained from the vector cross product).

It must be added that in the Plücker coordinate system a line is denoted by $\hat{l} = (\vec{m}, \vec{r})$. The intersection point $\boldsymbol{P}$ of two lines ($\vec{m}_1$, $\vec{r}_1$) and ($\vec{m}_2$, $\vec{r}_2$) is expressed by

$$\begin{aligned} \boldsymbol{P} &= \vec{r}_1 \times \vec{m}_1 + ((\vec{r}_2 \times \vec{m}_2)\vec{r}_1) \cdot \vec{r}_1 \\ &= \vec{r}_2 \times \vec{m}_2 + ((\vec{r}_1 \times \vec{m}_1)\vec{r}_2) \cdot \vec{r}_2. \end{aligned} \tag{5}$$

Let $\hat{l}_R$ denote any line (in this case it is an axis). After applying rigid body transformations, this line using the dual quaternions form is expressed by (Mukundan, 2002; Tan and Balchen, 1993)

$${}^{1n}\hat{l}_R = \hat{\boldsymbol{q}}_n \circ \hat{l}_R \circ \hat{\boldsymbol{q}}^*_{1n}, \tag{6}$$

where $\hat{\boldsymbol{q}}_{1n} = \hat{\boldsymbol{q}}_1 \circ \hat{\boldsymbol{q}}_2 \circ \cdots \circ \hat{\boldsymbol{q}}_n$ and n is the number of transformations, e.g., $\hat{\boldsymbol{q}}_{12}$ denotes the transformation obtained by the two first degrees of freedom.

Let us assume that $\boldsymbol{P}$ is the end-effector point (the intersection point of the X, Y, Z axes of the end-effector coordinates system). Based on Eqns. (5) and (6) and using the definition of the dual quaternion, this intersection point $\boldsymbol{P}$ is expressed by

$$\begin{aligned} \boldsymbol{P} = \boldsymbol{VR}\{{}^{1n}\hat{l}_x\} \times \boldsymbol{VR}\{{}^{1n}\hat{l}_x\} + ((\boldsymbol{VR}\{{}^{1n}\hat{l}_z\} \\ \times \boldsymbol{VD}\{{}^{1n}\hat{l}_z\}) \cdot \boldsymbol{VR}\{{}^{1n}\hat{l}_x\}) \cdot \boldsymbol{VR}\{{}^{1n}\hat{l}_x\}. \end{aligned} \tag{7}$$

Note that the intersection point of each pair of three axes is the intersection of the two axes as well; therefore, following (Ge *et al.*, 2018), in (7) just two axes are considered, namely, X and Z.

3. New sub-problem solution and a general formula

3.1. Solving inverse kinematics using a sub-problem. The classical Paden–Kahan sub-problems describing kinematic transformations are (i) rotation about a

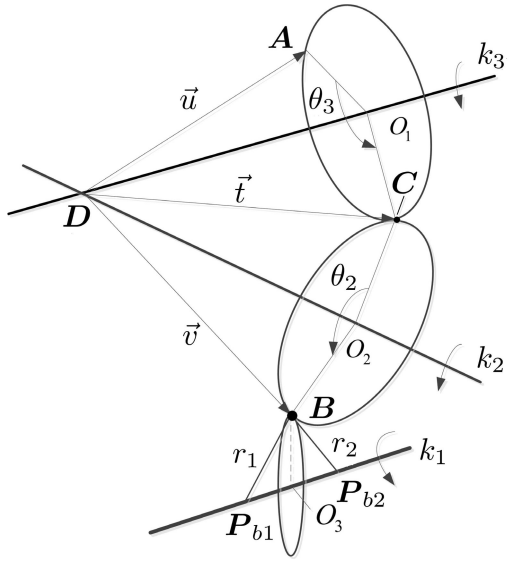

Fig. 1. Structure of the new sub-problem.

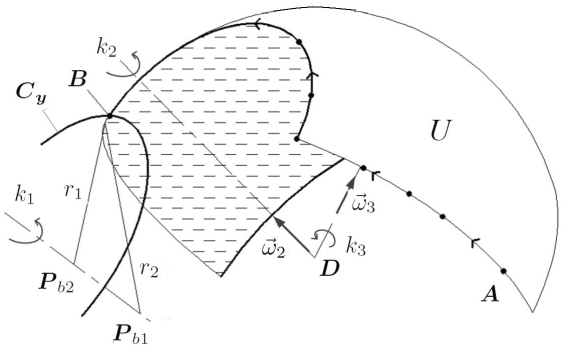

Fig. 2. Structure of the extended sub-problem.

single axis, (ii) rotation about two subsequent axes, (iii) rotation by a given amount. The decoupling is introduced by selecting special points, such as (a) the point on the axis and (b) the intersection point of two or more axes (Murray, 1994). The inverse kinematics problem can be converted into such sub-problems accordingly. Unfortunately, the existing methods for Paden–Kahan sub-problems solution cannot be applied to all configurations. Therefore a new sub-problem formulation was introduced. It is based on the second Paden–Kahan sub-problem, which is a point rotation around two intersecting axes for a given amount. With two known rotations of such a point around two intersecting axes and with one more rotation around a separated axis, this problem is equivalent to the 3R situation.

3.2. General description of kinematic transformations using dual quaternions. A key for solving the inverse kinematics problem by using sub-problems is to divide the configuration into appropriate parts (sub-problems). Sometimes, when solving the inverse kinematics problem using screw theory, the Plücker coordinate system is applied. The dual quaternion is another possible representation leading to a computationally efficient solution. The general formula describing kinematic transformations based on dual quaternions and Plücker coordinates is the following:

$$\begin{aligned} r_1 &= \Big\| \Big(\boldsymbol{VR}\{^{12}\hat{l}_2\} \times \boldsymbol{VR}\{^{12}\hat{l}_2\} + ((\boldsymbol{VR}\{^{12}\hat{l}_1\} \\ &\quad \times \boldsymbol{VD}\{^{12}\hat{l}_1\}) \cdot \boldsymbol{VR}\{^{12}\hat{l}_2\}) \cdot \boldsymbol{VR}\{^{12}\hat{l}_2\} \Big) - \boldsymbol{P}_{b1} \Big\|, \\ r_2 &= \Big\| \Big(\boldsymbol{VR}\{^{12}\hat{l}_2\} \times \boldsymbol{VR}\{^{12}\hat{l}_2\} + ((\boldsymbol{VR}\{^{12}\hat{l}_1\} \\ &\quad \times \boldsymbol{VD}\{^{12}\hat{l}_1\}) \cdot \boldsymbol{VR}\{^{12}\hat{l}_2\}) \cdot \boldsymbol{VR}\{^{12}\hat{l}_2\} \Big) - \boldsymbol{P}_{b2} \Big\|, \end{aligned} \tag{8}$$

where r_1 and r_2 are distances from $\boldsymbol{P}$ to $\boldsymbol{P}_{b1}$ and to $\boldsymbol{P}_{b2}$, and $^{12}\hat{l}_i$ denotes the axes after two transformations. Taking into account the norm of the left-hand part of the equations above, the distance from the end-effector to the points $\boldsymbol{P}_{b1}$, $\boldsymbol{P}_{b2}$ after the 2DOF transformation is obtained (Murray, 1994).

The formula concerns the case when two lines $\hat{l_1}$ and $\hat{l_2}$ intersect at point $\boldsymbol{P}$ which rotates around the two subsequent axes of the kinematic structure, reaching a new position. $\boldsymbol{P}_{b1}$ and $\boldsymbol{P}_{b2}$ are arbitrarily selected points; they create an axis in the 3D space. The initial and end positions of the rotated point are known; the distances from the end positions to $\boldsymbol{P}_{b1} = [x_{b1}, y_{b1}, z_{b1}]$ and $\boldsymbol{P}_{b2} = [x_{b2}, y_{b2}, z_{b2}]$ $(\boldsymbol{P}_{b1} \neq \boldsymbol{P}_{b2})$ are denoted by r_1 and r_2 respectively.

Some special cases are the following:

(i) if the new position overlaps with $\boldsymbol{P}_{b1}$ and $\boldsymbol{P}_{b2}$, then distances r_1 and r_2 are zero;

(ii) if the point is rotated around only one axis to the new position, the distance between this new position and point $\boldsymbol{P}_b$ is expressed by r, and there will be only one equation in (8);

(iii) if the point is rotated around only one axis to a new position, and the new position overlaps with $\boldsymbol{P}_b$, there will be only one equation in (8) and the distance r will be zero.

Using (8) for multi-DOF manipulator analysis, the kinematic structure is divided into several parts. The method is applied separately to each part.

3.3. Definition and solution of the new sub-problem. The aim of introducing the new sub-problem is to simplify the inverse kinematics analysis. The new

sub-problem considered in this paper concerns a 3R case with two rotations around two intersecting axes and one more rotation around a separated axis (see Fig. 1). It is an extension of the Paden–Kahan sub-problem. Solving this problem, the dual quaternions approach with geometric transformations was applied. Section 4 illustrates how the inverse kinematics problem is solved using dual quaternions, considering the 3R transformation introduced above.

Let us consider point $\boldsymbol{C}$ located at the intersection of two circles denoting the revolutions around two intersecting axes k_3, k_2 (Fig. 1). Getting the position of $\boldsymbol{C}$ in the base reference frame is a key point of the new sub-problem. After position $\boldsymbol{C}$ is obtained, the 3R problem will be further divided into the 1st Paden–Khan sub-problem and the 2nd Paden–Khan sub-problem. As illustrated in Fig. 1, rotation axes k_2 and k_3 intersect at point $\boldsymbol{D}$; $\vec{u} = \boldsymbol{A} - \boldsymbol{D}$ is the vector between points $\boldsymbol{A} = [x_A, y_A, z_A]$ and $\boldsymbol{D}$, $\vec{v} = \boldsymbol{B} - \boldsymbol{D}$ is the vector between points $\boldsymbol{B} = [x_B, y_B, z_B]$ and $\boldsymbol{D}$, and finally $\vec{t} = \boldsymbol{C} - \boldsymbol{D}$ is the vector between points $\boldsymbol{C} = [x_C, y_C, z_C]$ and $\boldsymbol{D} = [x_D, y_D, z_D]$.

Figure 2 illustrates the workspace for the revolute motion around two axes. For analysis of this situation, only the position of point $\boldsymbol{C}$ is needed. As the figure shows, the point-winding rotation of point $\boldsymbol{A}$ is part of a circle. The motion of $\boldsymbol{A}$ rotating by angle θ_3 around k_3 forms an arc, which rotates around k_2 by angle θ_2 forming a surface. This surface is the workspace of the 2DOF manipulator (Fig. 3).

Point $\boldsymbol{B}$ (see Fig. 1) is the final point of a serial kinematic structure. This point was reached by rotation θ_1 around the k_1 axis forming an arc (Fig. 2) which is part of the circle $\boldsymbol{C_y}$. The position of point $\boldsymbol{B}$ on the circle $\boldsymbol{C_y}$ is determined by intersecting spheres centered in $\boldsymbol{P}_{b1}$ and $\boldsymbol{P}_{b2}$ with radiuses r_1 and r_2 respectively, (Fig. 1). In other words, circle $\boldsymbol{C_y}$ is created by the intersection of the following spheres:

$$\begin{aligned}(x - x_{b1})^2 + (y - y_{b1})^2 + (z - z_{b1})^2 &= r_1^2,\\ (x - x_{b2})^2 + (y - y_{b2})^2 + (z - z_{b2})^2 &= r_2^2.\end{aligned} \tag{9}$$

Finally, the position of point $\boldsymbol{B}$ is obtained as the intersection of circle $\boldsymbol{C_y}$ with workspace $\boldsymbol{U}$—the surface produced by the motion of point $\boldsymbol{A}$ as illustrated in Fig. 2 and addressed as the workspace of 2DOF manipulator.

As illustrated in Fig. 1, rotation axes k_2 and k_3 intersect. The vectors $\vec{u}$, $\vec{v}$, $\vec{t}$ expressed by $\hat{u}$, $\hat{v}$, $\hat{t}$ in the dual quaternions notation conform to the following equation:

$$\hat{\boldsymbol{q}}_1 \circ \hat{u} \circ \hat{\boldsymbol{q}}_1^* = \hat{t} = \hat{\boldsymbol{q}}_2 \circ \hat{v} \circ \hat{\boldsymbol{q}}_2^*. \tag{10}$$

The vectors $\vec{\omega}_3 = [r_{x3}, r_{y3}, r_{z3}]$, $\vec{\omega}_2 = [r_{x2}, r_{y2}, r_{z2}]$ are the direction vectors of k_3 and k_2 (Fig. 1). Since $\vec{\omega}_3$ ($\hat{\omega}_3$ in quaternion form), $\vec{\omega}_2$ ($\hat{\omega}_2$ in quaternion form) and $\vec{\omega}_3 \times \vec{\omega}_2$, are linearly independent, we have

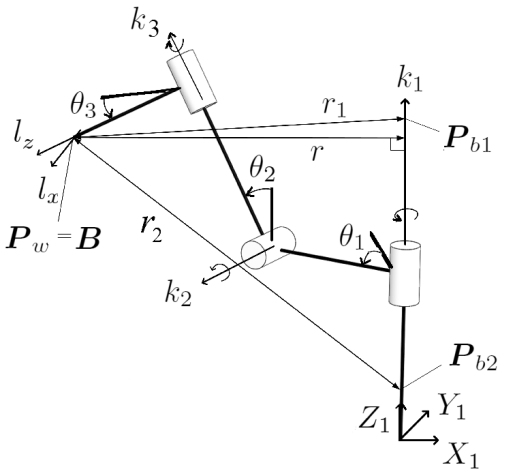

Fig. 3. Kinematic structure considered as a sub-problem in the described method.

$$\begin{aligned}\hat{t} &= e_1\hat{\omega}_3 + e_2\hat{\omega}_2 + e_3[0, \boldsymbol{VR}\{\hat{\omega}_3 \circ \hat{\omega}_2\}], \qquad (11)\\ e_1 &= \frac{SR\{\hat{\omega}_3 \circ \hat{\omega}_2\}SR\{\hat{\omega}_2 \circ \hat{u}\} - SR\{\hat{\omega}_3 \circ \hat{v}\}}{SR\{\hat{\omega}_3 \circ \hat{\omega}_2\}^2 - 1},\\ e_1 &= \frac{SR\{\hat{\omega}_3 \circ \hat{\omega}_2\}SR\{\hat{\omega}_3 \circ \hat{v}\} - SR\{\hat{\omega}_2 \circ \hat{u}\}}{SR\{\hat{\omega}_3 \circ \hat{\omega}_2\}^2 - 1},\\ e_3 &= \sqrt{\frac{\|\hat{u}\|^2 - \alpha^2 - \beta^2 - 2\alpha\beta \cdot SR\{\hat{\omega}_3 \circ \hat{\omega}_2\}}{\|\boldsymbol{VR}\{\hat{\omega}_3 \circ \hat{\omega}_2\}\|^2}}.\end{aligned}$$

Solving the above formulas, the coordinates of point $\boldsymbol{B}$, which denotes point $\boldsymbol{A}$ after rotation, were obtained. Then the approach of the 1st Paden–Kahan sub-problem obtaining θ_3 was used,

$$\theta_3 = \operatorname{atan2}[SR\{\hat{\omega}_3 \circ \hat{u}' \circ \hat{t}'\}, SR\{\hat{u}' \circ \hat{t}'\}], \tag{12}$$

where $\hat{u}' = \hat{u} - SR\{\hat{\omega}_3 \circ \hat{u}\} \cdot \hat{\omega}_3$, $\hat{t}' = \hat{\boldsymbol{q}} \circ \hat{u} \circ \hat{\boldsymbol{q}}^* - SR\{\hat{\omega}_3 \circ \hat{\boldsymbol{q}} \circ \hat{u} \circ \hat{\boldsymbol{q}}^*\} \cdot \hat{\omega}_3$, $\hat{\boldsymbol{q}} = [\cos(\theta_3/2), \sin(\theta_3/2) \cdot \hat{\omega}_3]$.

3.4. Summary. A new sub-problem is expressed by Eqn. (8) which is used for solving the 3R inverse problem (the current sub-problems are only used for solving 2R and 1R cases). The new sub-problem can be applied to any 3DOF system extracted from a more complex serial chain with revolute joints. The steps for solving the inverse kinematics problem are as follows:

Step 1. Select the intersecting point of up to three joint axes starting from the end of the kinematic chain (from the wrist). Produce kinematic equations for the remaining axes (excluding the part extracted by intersection). The structure considered is decoupled into two parts.

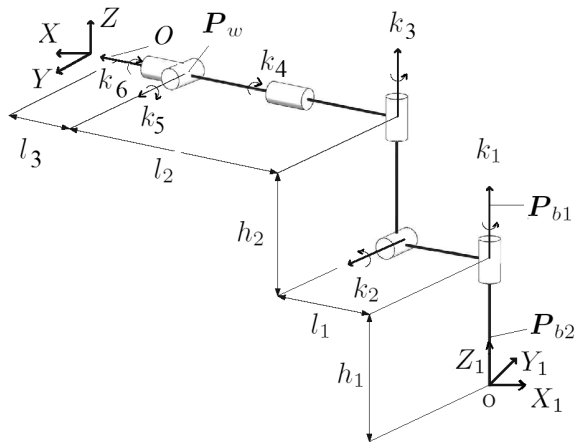

Fig. 4. 6R manipulator in its reference configuration.

Step 2. Select two points on the first axis of the starting structure and construct the equation describing the distance from the two points of this axis to the intersection point identified in Step 1. This equation is expressed by (8). By obtaining the distance from these two points to the intersection point, the revolute axes for the first part of the structure are obtained using Eqn. (6).

Step 3. After the angles are obtained in Step 2, the new kinematic equation is acquired. If needed, Steps 1 and 2 are repeated.

4. Case studies: Kinematics of a 6DOF serial manipulator

4.1. Introduction to the problem. The presented example should be seen as a case study illustrating the method. The 6DOF structure was chosen because it can be easily analyzed using also other methods, thus enabling easy validation of the method with the other ones.

In the described case the structure of a 6DOF manipulator was divided into two 3DOF parts. Then each 3R problem was solved without further division. As will be shown, the computation load is here smaller than in the other solution (i.e., a solution obtained with the D–H method). Moreover, the singularity problem does not arise.

4.2. Forward kinematics based on dual quaternions. First (X_1,Y_1,Z_1) is the base reference frame, the joint direction vectors are defined in this frame (Fig.4) while the direction axes of all joints are described by

$$\begin{aligned} &\vec{l}_1 = [0,0,1]^{\mathrm{T}}, \quad \vec{l}_2 = [1,0,0]^{\mathrm{T}}, \quad \vec{l}_3 = [0,0,1]^{\mathrm{T}}, \\ &\vec{l}_4 = [0,1,0]^{\mathrm{T}}, \quad \vec{l}_5 = [1,0,0]^{\mathrm{T}}, \quad \vec{l}_6 = [0,1,0]^{\mathrm{T}}. \end{aligned} \tag{13}$$

Next, some points located on the main axes of reference frames are selected:

$$\begin{aligned} &\boldsymbol{P}_1 = [0,0,z_{p1}], \quad \boldsymbol{P}_2 = [0,y_{p2},z_{p2}], \\ &\boldsymbol{P}_3 = [0,y_{p3},z_{p3}], \quad \boldsymbol{P}_4 = [0,y_{p4},z_{p4}], \\ &\boldsymbol{P}_5 = [0,y_{p3},z_{p5}], \quad \boldsymbol{P}_6 = [0,y_{p6},z_{p6}], \end{aligned} \tag{14}$$

where $\boldsymbol{P}_1 \neq \boldsymbol{P}_2 \neq \boldsymbol{P}_3 \neq \boldsymbol{P}_4 \neq \boldsymbol{P}_5 \neq \boldsymbol{P}_6$. The point coordinates take the following values:

$$\begin{aligned} &y_{p2} = l_1, \quad y_{p3} = y_{p2}, \quad y_{p4} = y_{p1} + l_2, \\ &y_{p5} = y_{p4}, \quad y_{p6} = y_{p5}, \\ &z_{p1} = h_1, \quad z_{p2} = z_{p1}, \quad z_{p3} = z_{p1} + h_2, \\ &z_{p4} = z_{p3}, \quad z_{p5} = z_{p3}, \quad z_{p6} = z_{p3}. \end{aligned} \tag{15}$$

The moment vectors for all axes are expressed by

$$\vec{m}_i = \boldsymbol{P}_i \times \vec{l}_i, \quad (i = 1, \ldots, 6). \tag{16}$$

Equation (6) allows us to deliver the location of the X and Y axes associated with the end-effector point (Fig. 3). This location is expressed using the dual quaternions formalism and considering that the end-effector performs linear motion:

$$\begin{aligned} \hat{l}'_x &= \boldsymbol{l}'_x + \varepsilon \boldsymbol{l}'^o_x \\ &= \hat{\boldsymbol{q}}_{16} \circ \boldsymbol{l}_x \circ \hat{\boldsymbol{q}}^*_{16} = \hat{\boldsymbol{q}}_{16} \circ (\boldsymbol{l}_x + \varepsilon \boldsymbol{l}^o_x) \circ \hat{\boldsymbol{q}}^*_{16}, \\ \hat{l}'_z &= \boldsymbol{l}'_z + \varepsilon \boldsymbol{l}'^o_z \\ &= \hat{\boldsymbol{q}}_{16} \circ \boldsymbol{l}_z \circ \hat{\boldsymbol{q}}^*_{16} = \hat{\boldsymbol{q}}_{16} \circ (\boldsymbol{l}_z + \varepsilon \boldsymbol{l}^o_z) \circ \hat{\boldsymbol{q}}^*_{16}. \end{aligned} \tag{17}$$

By referring to the relation (7), the position of the end-effector was obtained:

$$\begin{aligned} \boldsymbol{P} = \boldsymbol{VR}\{^{16}\hat{l}'_x\} \times \boldsymbol{VR}\{^{16}\hat{l}'_x\} + ((\boldsymbol{VR}\{^{16}\hat{l}'_z\} \\ \times \boldsymbol{VD}\{^{16}\hat{l}'_z\}) \cdot \boldsymbol{VR}\{^{16}\hat{l}'_x\}) \cdot \boldsymbol{VR}\{^{16}\hat{l}'_x\}, \end{aligned} \tag{18}$$

where $\boldsymbol{VR}\{^{16}\hat{l}'_x\}$, $\boldsymbol{VR}\{^{16}\hat{l}'_z\} \times \boldsymbol{VR}\{^{16}\hat{l}'_x\}$ and $\boldsymbol{VR}\{^{16}\hat{l}'_z\}$ are the directions of the X, Y and Z axes of the end-effector coordinate system.

4.3. Inverse kinematics based on dual quaternions. The inverse kinematics problem delivers each joint angle according to the known position of the end-effector. The problem is decoupled using the points on the axes (including the intersection point) (Sariyildiz and Temeltas, 2012). A complete kinematic structure is converted to appropriate sub-problems. This is done as follows:

Step 1. Origin $\boldsymbol{O}$ of the end-effector coordinate system is known together with the directions of the X, Y, Z axes. The intersection point $\boldsymbol{P}_w$ of the last three rotation axes of the manipulator is known. The rotation axis k_6 coincides with the X axis of the final coordinate system (end-effector system). Moreover, the location of $\boldsymbol{P}_w$ is such that $\boldsymbol{P}_w = \boldsymbol{P} - \vec{l}_x \cdot l_3$, where $\vec{l}_x$ is the direction of the X axis in the end-effector coordinate system and l_3 is the link length (Fig. 4). Since $\boldsymbol{P}_w$ is the intersection point of the three axes, the rotation of the three last degrees of

freedom does not affect the position of this point. Let us denote by $\boldsymbol{A}$ the initial position of the origin of the wrist joint (see Figs. 1 and 4). After the manipulator motion, this point is transformed to point $\boldsymbol{B}$ (according to Fig. 1). The position of this intersection point is not affected by the last three axes, therefore we consider firstly the kinematics equations of the first three axes. It means that the 6DOF structure is decoupled into a 3R problem:

$$\begin{aligned}\boldsymbol{P}_w = \boldsymbol{VR}\{^{123}\hat{l}_6\} \times \boldsymbol{VR}\{^{123}\hat{l}_6\} + ((\boldsymbol{VR}\{^{123}\hat{l}_5\} \\ \times \boldsymbol{VD}\{^{123}\hat{l}_5\}) \cdot \boldsymbol{VR}\{^{123}\hat{l}_6\}) \cdot \boldsymbol{VR}\{^{123}\hat{l}_6\}.\end{aligned} \tag{19}$$

Step 2. The initial position of the wrist joint is $\boldsymbol{P}_w$, after the manipulator motion, the distance r from point $\boldsymbol{P}_w$ to axis k_1 is equal to the distance between $\boldsymbol{A}$ and $\boldsymbol{O}_3$. Moreover, the position of the wrist point is $\boldsymbol{A}$ (Fig. 1). The distances $\boldsymbol{P}_w$ from $\boldsymbol{P}_{b1}$, $\boldsymbol{P}_{b2}$ are r_1 and r_2, respectively. $\boldsymbol{P}_w$ was rotated by an angle of θ_3 around axis k_3, and then rotation θ_2 around axis k_2 was performed ($\boldsymbol{B}$ in Fig. 1). Using the new sub-problem, the distances r_1 and r_2 from $\boldsymbol{P}_w$ (point marking the wrist joint) to $\boldsymbol{P}_{b1}$ and $\boldsymbol{P}_{b2}$ are obtained:

$$\begin{aligned}r_1 = \Big\| \Big(\boldsymbol{VR}\{^{123}\hat{l}_6\} \times \boldsymbol{VR}\{^{123}\hat{l}_6\} + ((\boldsymbol{VR}\{^{123}\hat{l}_5\} \\ \times \boldsymbol{VD}\{^{123}\hat{l}_5\}) \cdot \boldsymbol{VR}\{^{123}\hat{l}_6\}) \\ \cdot \boldsymbol{VR}\{^{123}\hat{l}_6\} \Big) - \boldsymbol{P}_{b1} \Big\|, \\ r_2 = \Big\| \Big(\boldsymbol{VR}\{^{123}\hat{l}_6\} \times \boldsymbol{VR}\{^{123}\hat{l}_6\} + ((\boldsymbol{VR}\{^{123}\hat{l}_5\} \\ \times \boldsymbol{VD}\{^{123}\hat{l}_5\}) \cdot \boldsymbol{VR}\{^{123}\hat{l}_6\}) \\ \cdot \boldsymbol{VR}\{^{123}\hat{l}_6\} \Big) - \boldsymbol{P}_{b2} \Big\|.\end{aligned} \tag{20}$$

Points $\boldsymbol{P}_{b1}$ and $\boldsymbol{P}_{b2}$ are located on axis k_1, which means that the rotation of the k_1 axis does not influence the lengths of r_1 and r_2. Therefore, axis k_1 is not involved when expressing r_1 and r_4 (the rotation angle vanishes), and Eqns. (20) take the following form:

$$\begin{aligned}r_1 = \Big\| \Big(\boldsymbol{VR}\{^{23}\hat{l}_6\} \times \boldsymbol{VR}\{^{23}\hat{l}_6\} \\ + ((\boldsymbol{VR}\{^{23}\hat{l}_5\} \boldsymbol{VD}\{^{23}\hat{l}_5\}) \cdot \boldsymbol{VR}\{^{23}\hat{l}_6\}) \\ \cdot \boldsymbol{VR}\{^{23}\hat{l}_6\} \Big) - \boldsymbol{P}_{b1} \Big\|, \\ r_2 = \Big\| \Big(\boldsymbol{VR}\{^{23}\hat{l}_6\} \times \boldsymbol{VR}\{^{23}\hat{l}_6\} \\ + ((\boldsymbol{VR}\{^{23}\hat{l}_5\} \boldsymbol{VD}\{^{23}\hat{l}_5\}) \cdot \boldsymbol{VR}\{^{23}\hat{l}_6\}) \\ \cdot \boldsymbol{VR}\{^{23}\hat{l}_6\} \Big) - \boldsymbol{P}_{b2} \Big\|.\end{aligned} \tag{21}$$

Equation (21) has the same form as (8). Equations (4) and (21) are used for obtaining θ_2 and θ_3. It is the solution of introduced new sub-problem (see Section 3.3). After getting θ_2 and θ_3, Eqn. (19) is considered and, based on the 1st Paden–Kahan sub-problem, θ_1 is obtained. Here point $\boldsymbol{P}_w$ was rotated by an angle of θ_3 around axis k_3, and next rotation θ_2 around axis k_2 was performed (Sariyildiz *et al.*, 2011).

Step 3. The end-effector of the manipulator is rotated and its coordinates are obtained using the formula

$$\begin{aligned}\boldsymbol{P} = \boldsymbol{VR}\{^{45}\hat{l}'_z\} \times \boldsymbol{VR}\{^{45}\hat{l}'_z\} + ((\boldsymbol{VR}\{^{45}\hat{l}'_x\} \\ \times \boldsymbol{VD}\{^{45}\hat{l}'_x\}) \cdot \boldsymbol{VR}\{^{45}\hat{l}'_z\}) \cdot \boldsymbol{VR}\{^{45}\hat{l}'_z\},\end{aligned} \tag{22}$$

where $\hat{l}'_x = \hat{\boldsymbol{q}}_{13} \circ \hat{l}_x \circ \hat{\boldsymbol{q}}^*_{13}$, $\hat{l}'_z = \hat{\boldsymbol{q}}_{13} \circ \hat{l}_z \circ \hat{\boldsymbol{q}}^*_{13}$.

Equation (22) describes a special situation of the new sub-problem, which was introduced in the previous section. Here the point was rotated around axis k_5 by θ_5, and next rotated by θ_4 around axis k_4; the distances from the specified points $\boldsymbol{P}_{b3}$ and $\boldsymbol{P}_{b4}$ to the selected point on k_6, are r_3 and r_4. Axes k_4, k_5, k_6 intersect at the wrist joint. Points $\boldsymbol{P}_{b3}$ and $\boldsymbol{P}_{b4}$ overlap, and therefore r_3, r_4 are equal to zero. When angles θ_1, θ_2, θ_3, θ_4, θ_5 are known, θ_6 can be obtained. An arbitrarily selected point in the tool coordinate system is described by $\boldsymbol{P}_d = \boldsymbol{P} + \lambda d$. Now it is assumed that the two imaginary axes cross at this point; their direction vectors are $\vec{\omega}_7 = [0, 1, 0]^{\mathrm{T}}$, $\vec{\omega}_8 = [1, 0, 0]^{\mathrm{T}}$,

$$\begin{aligned}\boldsymbol{P}_d = \boldsymbol{VR}\{^{6}\hat{l}'_8\} \times \boldsymbol{VR}\{^{6}\hat{l}'_8\} + ((\boldsymbol{VR}\{^{6}\hat{l}'_7\} \\ \times \boldsymbol{VD}\{^{6}\hat{l}'_7\}) \cdot \boldsymbol{VR}\{^{6}\hat{l}'_8\}) \cdot \boldsymbol{VR}\{^{6}\hat{l}'_8\},\end{aligned} \tag{23}$$

where $\hat{l}'_7 = \hat{\boldsymbol{q}}_{15} \circ \hat{l}_7 \circ \hat{\boldsymbol{q}}^*_{15}$, $\hat{l}'_8 = \hat{\boldsymbol{q}}_{15} \circ \hat{l}_8 \circ \hat{\boldsymbol{q}}^*_{15}$ and θ_6 can be obtained using (23).

So far, six joint angles $\theta_1, \ldots, \theta_6$ of the manipulator have been obtained. It must be noted that in the considered example the final three joint axes intersect. Out of the first three joint axes, the second and the third intersect, too. When this method is used for another kinematic structure, the inverse kinematics problem must be solved by a proper combination of the first and second type of sub-problems.

5. Simulation results

The manipulator shown in Fig. 4 was taken as the testing example. The manipulator parameters are as follows: $h_1 = 500, h_2 = 160, l_1 = 400, l_2 = 450, l_3 = 150$.

The task was to move the end-effector point along two line segments and along an arc in the 3D space. The trajectory was divided into 50 equal parts addressed as the control steps. The term 'control step' is used referring to the work of real controllers. The controller applies the point trajectories described in the Cartesian space; this means that the trajectories are represented as a series of points. The time intervals separating these points are called control steps. They are the working steps of a lower level controller. In each step the lower level controller supervises concurrently the motion of all joints so that

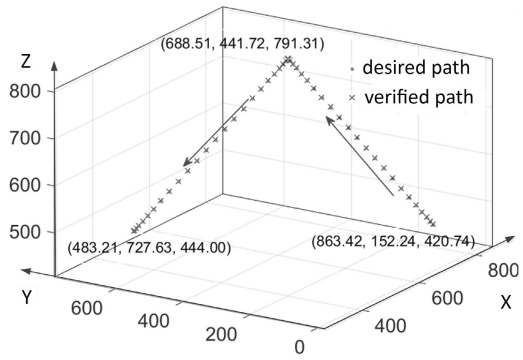

Fig. 5. Trajectory of the end-effector point: line segments. The path used for solving the inverse kinematics problem and the verified path given by the obtained joint trajectories after solving the direct kinematics problem are shown. Both paths overlap. The arrows present the motion direction.

the given point position is reached till the next motion demand concerning the next point. Figure 5 shows the 3D trajectory of the end-effector following the line segments. The trajectory starts at the point $(863.42, 152.24, 420.74)$ with intermediate point $(688.51, 441.72, 791.31)$ and the final position $(483.21, 727.63, 444.00)$. The coordinates are expressed in the robot base frame. For each point the inverse kinematics problem was solved. The obtained joint trajectories are shown in Fig. 6.

Figure 7 shows the arc-shaped trajectory of the end-effector from point $(835.16, -231.52, 660.95)$ to point $(298.85, 49.85, 1161.31)$. Figure 8 shows obtained joint trajectories. As seen in Figs. 6 and 8, the angular displacement of each joint is smooth, which indicates that not any calculation or numerical errors are involved. For completely checking the solutions to kinematics problems, the obtained joint trajectories were again used for solving the direct kinematics problem. The solution was delivering again the end-effector trajectory. The points of such trajectories are marked in Figs. 5 and 7 as the points of the verified path, while the points considered at the beginning are marked as the points of the initial path. As can be seen, the points of both trajectories are overlapping (within numerical accuracy, which will be commented upon bellow). discussed makes the proof of the correctness of the presented solution.

A comparison of the computational performance of different algebraic methods for a forward and an inverse kinematics problem is presented by Sariyildiz *et al*. (2011). The required number of operations, i.e., additions, subtractions, and multiplications for different algebraic methods, and varied complexity of

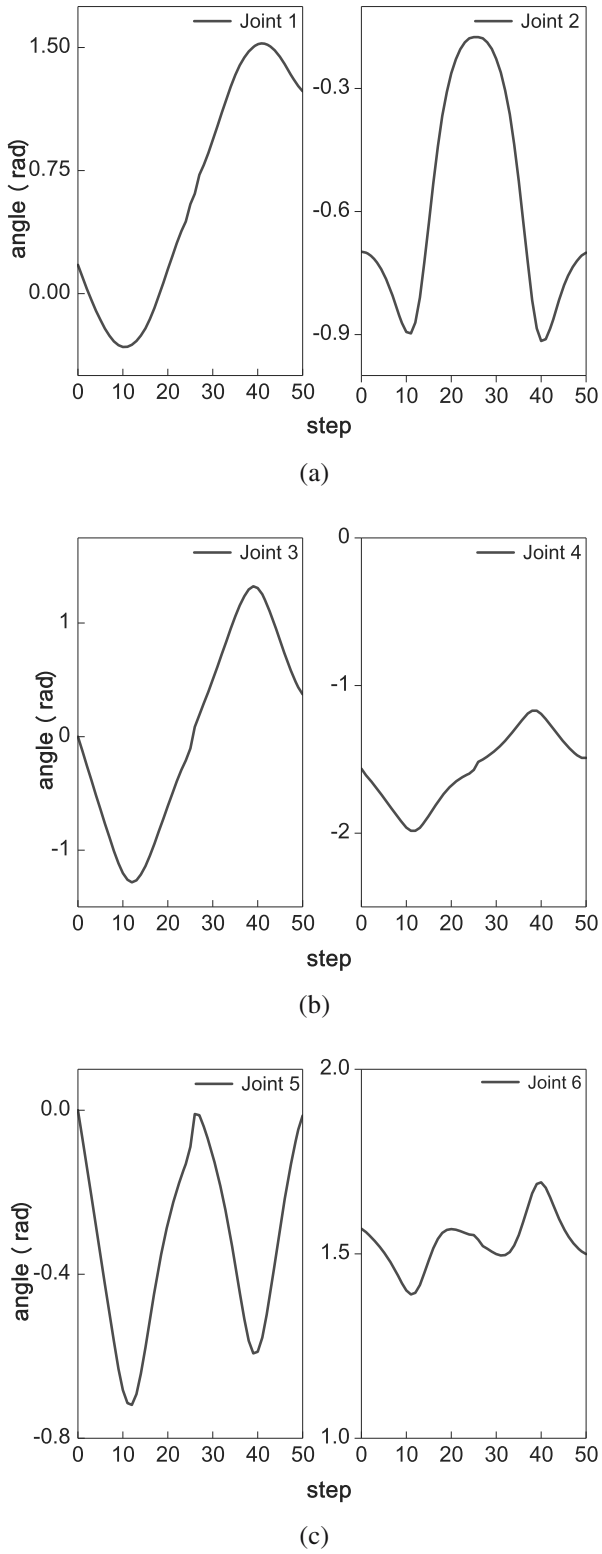

Fig. 6. Joint trajectories for the end-effector following the line segments.

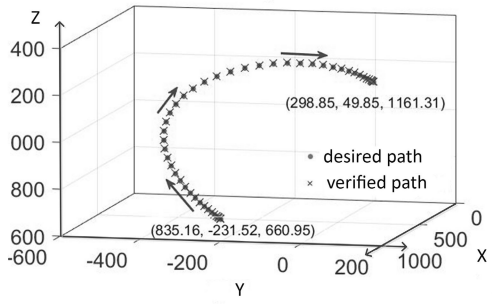

Fig. 7. Trajectory of the end-effector point: an arc path. The path used for solving the inverse kinematics problem and the verified path given by the obtained joint trajectories after solving the direct kinematics problem are shown. Both paths overlap. The arrows present the motion direction.

the discussed structure in terms of DOFs were analyzed, showing the disadvantage of the exponential mapping method as compared with the dual quaternions ones. In this paper, one of the methods used by Sariyildiz *et al*. (2011) was followed. The computation time was recorded when solving the direct kinematics problem from 1 up to 50 times (addressed as repetitions). The obtained computation time was next normalized to the repetition; this means that the overall time was divided by the number of repetitions involved. The dual quaternions method consumed less time, as illustrated in Fig. 9. Moreover, for dual quaternions, smaller variations in the computation time were also observed. The computation time was evaluated using MATLAB tic-toc commands on an Intel core i5-2450 Duo 2.2 GHz PC with 4 GB RAM.

6. Conclusions

Industrial robot controllers have limited computational power. In sensory-based control, when end-effector trajectories are modified, on-line joint coordinates must be obtained in real time (using formulas produced and implemented off-line). Moreover, in some control modes (e.g., human guided motion), the position of the end-effector must be recovered fast from joint coordinates. Therefore a very fast solution of the direct kinematics problem is needed, too. The conclusion that numerical efficiency of calculations is critical was the motivation for the presented research.

The new sub-problem is proposed for solving the inverse kinematics problem of kinematic structures for which the decomposition to Paden–Kahan sub-problems is not sufficient. The sub-problem concerns the 3R case while the current sub-problems considered only 2R and 1R cases. The presented method is general. It is based

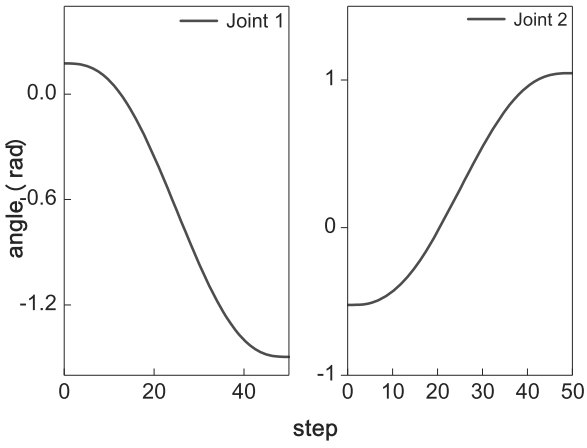

(a)

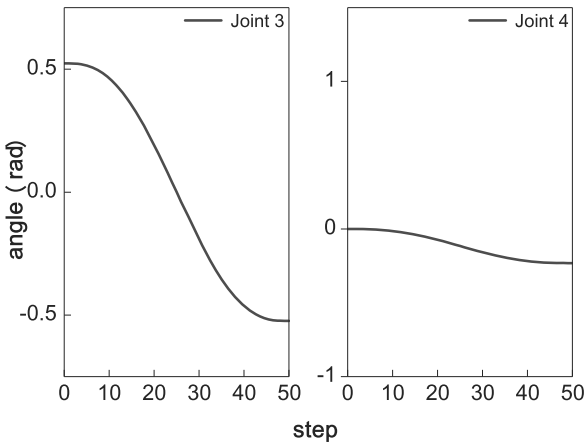

(b)

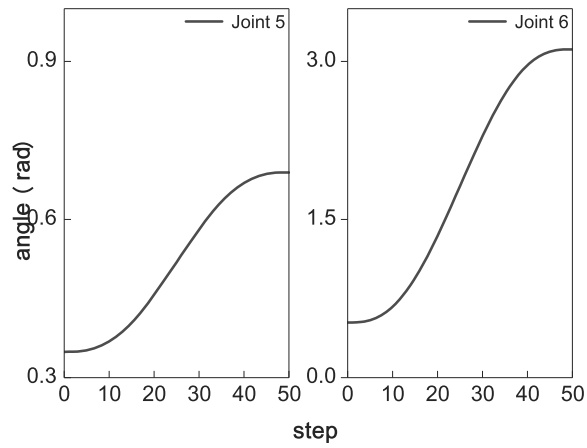

(c)

Fig. 8. Joint positions of the manipulator following an arc path.

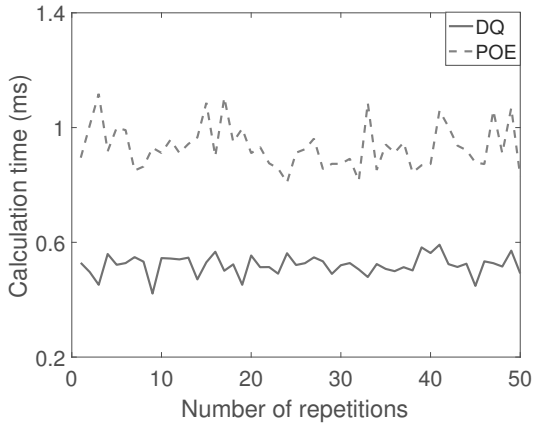

Fig. 9. Comparison of the computation load for the forward kinematics problem (DQ: dual quaternions method, POE: exponential product method).

on dual quaternions. Therefore it can be applied in any case where such methods can be used, particularly for all manipulators with revolute joints.

The presented case studies concerned only the end-effector position but its orientation was investigated. A relatively simple 6-DOF structure allows an easy comparison with the other solutions, making sure that the errors were not introduced due to problem complexity. It is the structure of a new manipulator that is currently under development. Therefore such studies were also needed for development work.

It must be noted that method validation using redundant structures would be difficult and problematic at this stage. In redundant structures, there can be several feasible configurations for the same end-effector paths. Moreover, comparisons with the other methods can be very troublesome due to serious difficulties in the implementation (especially considering the need for posture optimization and singularities avoidance in the other methods). Our further research plans include tests considering the end-effector orientation, and implementation of the obtained solutions in the developed manipulator controller. The next planned step is the modeling of robot dynamics using the dual quaternions concept.

Acknowledgment

The authors would like to express their gratitude to the National Key Research and Development Program of China (2017YFB1303304) and to the Tianjin Key Research and Development Plan of China (18YFFCTG00040 and 17ZXZNGX00110).

The work on this paper was supported by the Tianjin Municipality Foreign 1000 Talents Expert Program.

References

An, H.S., Lee, J.H., Lee, C., Seo, T. and Lee, J.W. (2017). Geometrical kinematic solution of serial spatial manipulators using screw theory, *Mechanism and Machine Theory* **116**: 404–418.

An, H.S., Seo, T.W. and Lee, J.W. (2018). Generalized solution for a sub-problem of inverse kinematics based on product of exponential formula, *Journal of Mechanical Science and Technology* **32**(5): 2299–2307.

Cariow, A., Cariowa, G. and Witczak, M. (2015). An FPGA-oriented fully parallel algorithm for multiplying dual quaternions, *Measurement Automation Monitoring* **61**(7): 370–372.

Chang, C., Liu, J., Ni, Z. and Qi, R. (2018). An improved kinematic calibration method for serial manipulators based on POE formula, *Robotica* **36**(8): 1244–1262.

Chen, Q., Zhu, S. and Zhang, X. (2015). Improved inverse kinematics algorithm using screw theory for a six-DOF robot manipulator, *International Journal of Advanced Robotic Systems* **12**(10): 1–9.

Clifford, W.K. (1882). *Mathematical Papers*, Macmillan and Company, London.

Craig, J.J. (2009). *Introduction to Robotics: Mechanics and Control, 3/E*, Pearson Education India, Delhi.

Ge, W., Chen, L., Wang, X., Xing, E. and Zielinska, T. (2019). Kinematics modeling and analysis of manipulator using the dual quaternion, *2019 IEEE International Conference on Mechatronics and Automation (ICMA), Tianjin, China*, pp. 750–755, DOI: 10.1109/ICMA.2019.8816603.

Ge, W., Yu, X. and Xing, E. (2018). Kinematics modeling and analysis of manipulator based on dual quaternion, *Journal of Mechanical Transmission* **42**(07): 112–117, DOI :10.16578/j.issn.1004.2539.2018.07.023.

Gouasmi, M., Ouali, M. and Brahim, F. (2012). Robot kinematics using dual quaternions, *IAES International Journal of Robotics and Automation* **1**(1): 13–30.

Gui, H. and Vukovich, G. (2016). Dual-quaternion-based adaptive motion tracking of spacecraft with reduced control effort, *Nonlinear Dynamics* **83**(1–2): 597–614.

Kenwrigth, B. (2013). Inverse kinematics with dual-quaternions, exponential-maps, and joint limits, *International Journal on Advances in Intelligent Systems* **6**(1): 53–65.

Kussaba, H.T.M., Figueredo, L.F.C., Ishihara, J.Y. and Adorno, B.V. (2017). Hybrid kinematic control for rigid body pose stabilization using dual quaternions, *Journal of the Franklin Institute: Engineering and Applied Mathematics* **354**(7): 2769–2787.

Mueller, A. (2017). Coordinate mappings for rigid body motions, *Journal of Computational and Nonlinear Dynamics* **12**(2): 1–13.

Mukundan, R. (2002). Quaternions: From classical mechanics to computer graphics, and beyond, *Proceedings of the 7th Asian Technology Conference on Mathematics, Melaka, Malaysia*, pp. 97–105.

Murray, R.M. (1994). *A Mathematical Introduction to Robotic Manipulation*, CRC Press, Inc. Boca Raton, FL.

Oezguer, E. and Mezouar, Y. (2016). Kinematic modeling and control of a robot arm using unit dual quaternions, *Robotics and Autonomous Systems* **77**: 66–73.

Sariyildiz, E., Cakiray, E. and Temeltas, H. (2011). A comparative study of three inverse kinematic methods of serial industrial robot manipulators in the screw theory framework, *International Journal of Advanced Robotic Systems* **8**(5): 9–24.

Sariyildiz, E. and Temeltas, H. (2012). A new formulation method for solving kinematic problems of multiarm robot systems using quaternion algebra in the screw theory framework, *Turkish Journal of Electrical Engineering & Computer Sciences* **20**(4): 607–628.

Singh, A., Singla, E., Soni, S. and Singla, A. (2018). Kinematic modeling of a 7-degree of freedom spatial hybrid manipulator for medical surgery, *Proceedings of the Institution of Mechanical Engineers H: Journal of Engineering in Medicine* **232**(1): 12–23.

Tan, Q. and Balchen, J.G. (1993). General quaternion transformation representation for robotic application, *Proceedings of the IEEE Systems Man and Cybernetics Conference, Le Touquet, France,* Vol. 3, pp. 319–324.

Vidaković, J.Z., Lazarević, M.P., Kvrgić, V.M., Dančuo, Z.Z. and Ferenc, G.Z. (2014). Advanced quaternion forward kinematics algorithm including overview of different methods for robot kinematics, *FME Transactions* **42**(3): 189–198.

Wang, H., Lu, X., Sheng, C., Zhang, Z., Cui, W. and Li, Y. (2018). General frame for arbitrary 3R subproblems based on the POE model, *Robotics and Autonomous Systems* **105**: 138–145.

Wang, J.-Y., Liang, H.-Z., Sun, Z.-W., Wu, S.-N. and Zhang, S.-J. (2013). Relative motion coupled control based on dual quaternion, *Aerospace Science and Technology* **25**(1): 102–113.

Wang, X., Yu, C. and Lin, Z. (2012). A dual quaternion solution to attitude and position control for rigid-body coordination, *IEEE Transactions on Robotics* **28**(5): 1162–1170.

Xiong, G., Ding, Y., Zhu, L. and Su, C.-Y. (2017). A product-of-exponential-based robot calibration method with optimal measurement configurations, *International Journal of Advanced Robotic Systems* **14**(6): 1–11.

Yue-sheng, T. and Ai-Ping, X. (2008). Extension of the second Paden–Kahan sub-problem and its application in the inverse kinematics of a manipulator, *IEEE Conference on Robotics, Automation and Mechatronics, Chengdu, China*, pp. 379-381, DOI:10.1109/RAMECH.2008.4681401.

Zhao, R., Shi, Z., Guan, Y., Shao, Z., Zhang, Q. and Wang, G. (2018). Inverse kinematic solution of 6R robot manipulators based on screw theory and the paden-kahan subproblem, *International Journal of Advanced Robotic Systems* **15**(6): 1–11.

Zhu, C. and Zhao, Z. (2019). Research on influence of joint clearance on precision of 3-TPT parallel robot, *Mechanical Sciences* **10**(1): 287–298.

Lei Chen is studying for an MSc degree at the Tianjin Key Laboratory for Advanced Mechatronic System Design and Intelligent Control, Tianjin University of Technology. His research interests include kinematics and dynamic analysis of industrial robots, robot control and screw theory.

Teresa Zielinska received her MSc degree in automatic control and her PhD degree in robotics from the Warsaw University of Technology (WUT), Poland. In 1995, she obtained her postdoctoral (DSc) degree in biocybernetics from the Polish Academy of Sciences. She has been a senior member of the IEEE since 2005. Her research interests include design, motion synthesis and control of walking machines and humanoids. She has developed several robotics control systems, including kinematic studies. In recent years she has focused on biorobotics.

Jikun Wang received his MSc and PhD degrees from the Warsaw University of Technology, Faculty of Power and Aeronautical Engineering, Poland. He is employed at the Faculty of Mechatronics, Warsaw University of Technology, as an assistant professor. He has been a member of IFToMM, TC for Robotics and Mechatronics, since 2018. His research interests include biomechanics and robotics.

Weimin Ge obtained his MSc degree from the University of Science & Technology in Beijing (USTB). He received his PhD degree from Tianjin University, China. He is employed by the Tianjin University of Technology and acts as the deputy dean of the School of Mechanical Engineering. He focuses on robots and control technologies. Among other things, he has been engaged in projects devoted to research and applications of virtual reality and computer aided-technologies (CAD).

Received: 22 August 2019
Revised: 13 January 2020
Re-revised: 17 March 2020
Accepted: 26 March 2020